


Rethinking Model-Based Fault Detection: Uncertainties, Risks, and Optimization Based on a Multilevel Converter Case Study

Yantao Liao  and Yi Zhang , *Member, IEEE*

Abstract—This article presents a probabilistic framework for assessing uncertainty and failure risk in model-based fault detection (MBFD) of power electronic systems. The proposed methodology encompasses uncertainty factor selection, uncertainty propagation, risk assessment, sensitivity analysis, and the development of tailored solutions to optimize MBFD performance. By quantifying two types of misdiagnosis, the risk-of-failure of MBFD has been evaluated under diversely random conditions. In a detailed case study on a modular multilevel converter (MMC), the framework has analyzed five different methods and revealed that existing MBFD methods can have misdiagnosis rates up to 20% due to uncertainties. By identifying leading uncertainty factors and mitigating their impacts, we have reduced the misdiagnosis rate to below 0.4%. While the MMC case study exemplifies practical implementation, the framework's generality makes it applicable to optimize fault detection across diverse power electronics applications.

Index Terms—Disturbance observer (DOB), fault detection, modular multilevel converters (MMCs), uncertainty quantification.

I. INTRODUCTION

WITH the increasing utilization of power electronic converters in safety-critical applications [1], [2], [3], the failure of power electronic systems has become increasingly severe. Timely and robust fault detection is vital to mitigate risks and prevent catastrophic damages. Among various fault detection approaches [3], [4], model-based fault detection (MBFD) techniques are a preferred choice for power electronic applications because of their explicit physical interpretations of fault detection and leveraging existing sensors without additional hardware.

Existing studies of MBFD methods in power electronics often provide validations as having seemingly 100% accuracy of detecting faults [4], [5]. The inherent uncertainties and associated risks

Manuscript received 17 November 2023; revised 21 April 2024 and 14 June 2024; accepted 17 July 2024. Date of publication 24 July 2024; date of current version 11 September 2024. This work was supported by Innovation Fund Denmark (IFD) through the Project of Artificial Intelligence for Next-Generation Power Electronics (AI-Power). Recommended for publication by Associate Editor J. Hu and M. Meneghini. (*Corresponding author: Yi Zhang.*)

Yantao Liao is with the Department of Electrical Engineering, Southeast University, Nanjing 210018, China (e-mail: liaoyt@seu.edu.cn).

Yi Zhang is with AAU Energy, Aalborg University, 9220 Aalborg, Denmark (e-mail: yiz@ieee.org).

Data is publicly available in: <https://dx.doi.org/10.21227/04e7-qw72>.

Color versions of one or more figures in this article are available at <https://doi.org/10.1109/TPEL.2024.3433030>.

Digital Object Identifier 10.1109/TPEL.2024.3433030

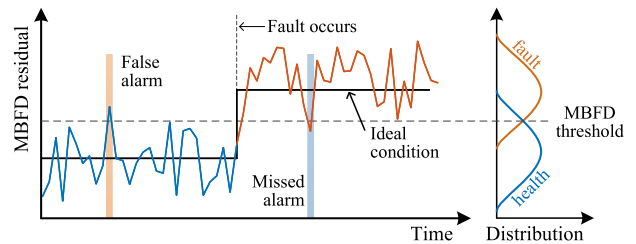
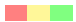


Fig. 1. Potential outcomes of practical MBFD. The solid black line represents the MBFD's residual under ideal conditions, while the colored line represents the residual with uncertainties.

TABLE I
RISK-OF-FAILURE OF FAULT DETECTIONS IN DIFFERENT APPLICATIONS

Applications	False alarm	Missed alarm	Reference
Renewable generation	33.3% – 62.5%	4.3% – 75.0%	[11], [12]
Power delivery	5.0% – 54.4%	10.0% – 20.0%	[13], [14]
Aircraft	1.0%	5.0%	[15]
Manufacture and motor	5.0%	38.0%	[16], [17]
Battery	0% – 62.0%	0% – 94.0%	[18]

Note: the risk of likelihood from high to low. 

have not received adequate attention [6]. For instance, notable contributions have been focused on advancing fault-detection functionalities [7], [8], [9], [10]. The robustness of these aforementioned studies has often been assessed by a few deterministic scenario tests that do not reflect to the stochastic nature of the system states. Besides, no information is provided regarding the risk-of-failure of their proposed methods. As a result, although their validations have revealed good effectiveness in a laboratory condition, their performances exposed to practical conditions are difficult to be guaranteed.

In practical applications, uncertainties significantly affect the performance of MBFD methods. As shown in Fig. 1, the detection of a fault appears straightforward under ideal conditions without uncertainties. However, practical implementations subject to various uncertainties can yield two risk-of-failure outcomes: *false alarm* and *missed alarm*. False alarms arise when the MBFD system incorrectly identifies a fault in the absence of any actual fault, resulting in operational disruptions [19]. Conversely, missed alarms occur when a fault remains undetected, introducing severe risks [15]. As listed in Table I,

the risk-of-failure of the fault detection has commonly existed in different applications. For example, an industrial report [11] highlighted numerous false alarms and up to 75% missed alarm in wind applications. From this perspective, failing to adequately assess uncertainties and associated risks renders the direct implementation of an MBFD method potentially hazardous instead of improving the system.

While uncertainties have been studied in design [20], [21] and reliability [2], [22] of power electronics, a noticeable gap regarding the uncertainties of MBFD is lacking an explicit assessment framework. To begin with, many existing MBFD studies [7], [9] tend to rely on a limited number of specific scenarios to conduct robustness testing and evaluate the impact of uncertainties. However, this approach is limited to revealing the full spectrum of issues arising from uncertainties. Furthermore, the aspects of uncertainty propagation and risk assessment in MBFD are often oversimplified, neglecting the coupling effects among different factors [7], [8], [23], [24]. As a result, their proposed solutions for mitigating risks associated with uncertainties frequently rely on manual and empirical methods [1], [10], [25], such as adding filters to reduce noise or adjusting fault-detection thresholds simply. A holistic consideration and systematic assessment of MBFD uncertainties are highly demanding.

In this article, we propose a risk-driven probabilistic framework to analyze the impact of multiple uncertainty factors in MBFD. The framework includes uncertainty factor selection, uncertainty propagation, risk assessment, sensitivity analysis, and optimization. Based on a modular multilevel converter (MMC), an existing MBFD method [7] for an insulate-gate bipolar transistor (IGBT) open-circuit fault is considered as a case study. The main contributions of this article are as follows.

- 1) The proposed uncertainty factor selection is based on explicit understandings of the system. The analysis reveals that the impact of uncertainties on the MBFD has two parts: dc bias and ac fluctuations. Different uncertainties are intricately coupled rather than independent.
- 2) To simultaneously consider multiple coupling effects among different uncertainties, a Monte Carlo analysis is employed. The risk-of-failure of the MBFD is defined as two contradictory error rates. It reveals that the conventional threshold adjustment is limited to improve the MBFD performance concerning these two error rates.
- 3) The sensitivity analysis enables to identify the leading uncertainty factor of the studied case. The subsequently proposed observer-enhanced method compensates this uncertainty, which simultaneously reduces the aforementioned two error rates of the MBFD method.

II. UNCERTAINTIES IN MBFD

MBFD approaches are based on comparing a measured signal, the actual plant output, with its estimated value derived from an explicit mathematical model of the system (see Fig. 2 top). Ideally, the difference, termed as the residual, should be zero when the system is healthy and deviate from zero when a fault is present. However, the actual residual of MBFD is inherently influenced by the following two categories of uncertainties.

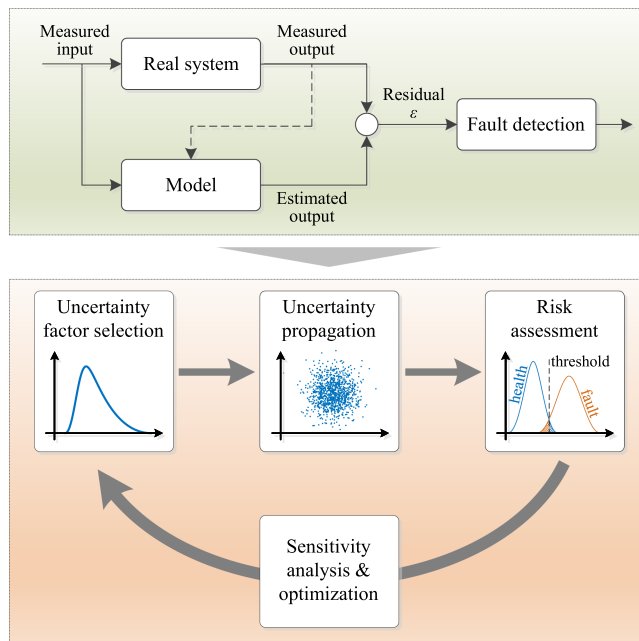


Fig. 2. MBFD (top) and a risk-driven probabilistic framework to analyze the impact of their uncertainties (bottom).

- 1) *Aleatory uncertainty*: It arises from the inherent variability or randomness in a system, which is often known as stochastic or irreducible uncertainty. Examples include noise in sensor measurements, natural variability in system properties, and random external influences.
- 2) *Epistemic uncertainty*: Stemming from incomplete knowledge about the system or potential errors in the model, this is referred to as reducible uncertainty. With providing more information or improving model accuracy, epistemic uncertainty can be minimized. Common examples include inaccuracies in model parameters and model simplifications, and other knowledge gaps.

In real-world systems, these two types of uncertainties are often coupled with each other. Traditional methods based on empirical and qualitative analyzes might not fully capture the diverse range of uncertainties or adequately facilitate their prioritization in addressing their impacts.

To address this challenge, this article introduces a risk-driven probabilistic framework for assessing uncertainties in MBFD. This method entails identifying potential uncertainties, prioritizing them based on quantified risks, and tackling the most relevant ones to ensure the MBFD at an acceptable risk level. The bottom of Fig. 2 shows a detailed flowchart of this process. Initially, uncertainty sources are identified comprehensively through a model analysis of MBFD. Subsequently, uncertainty propagation and two defined risk-of-failure metrics quantify the impact of each uncertainty on the MBFD performance. This quantification allows for the prioritization of uncertainties, facilitating the management of the most critical risks first. A more explicit case study and its optimization are elaborated upon in the subsequent sections.

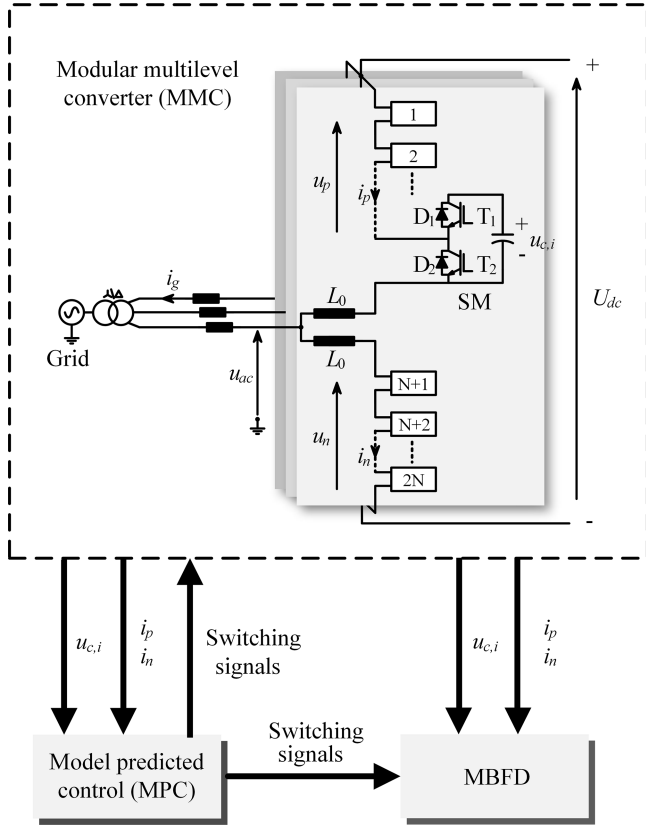


Fig. 3. Configuration of an MMC and an existing MBFD method [7] for open-circuit fault detection based on MPC.

III. MOTIVATION CASE STUDY OF THE MBFD AND THE ANALYTICAL IMPACT OF UNCERTAINTIES

In this section, an existing MBFD method [7] for the IGBT open-circuit fault of the MMC is utilized as a motivation case. Compared to the state-of-the-art, Zhou et al. [7] carried out excellent robustness tests to consider the impact of uncertainties. However, how to model uncertainties systematically and quantify their impacts remains unclear yet.

A. Configuration of the MMC and an Existing MBFD Method

A schematic of a three-phase MMC is shown in Fig. 3. Each phase of the MMC has two arms, where each arm consists of N series-connected half-bridge submodules (SMs) and an arm inductor L_0 (the upper and lower arm inductance are also denoted as L_p and L_n to consider their differences). Take phase a as an example and the subscript is neglected for simplification. The upper and lower arm currents and voltages are denoted as i_p , i_n , u_p , and u_n , respectively. The ac side current i_g and the circulating current i_{cir} are expressed as

$$\begin{cases} i_g = i_p - i_n \\ i_{cir} = \frac{i_p + i_n}{2}. \end{cases} \quad (1)$$

Each SM consists of two IGBTs with two antiparallel diodes and a capacitor. The two IGBTs are controlled with complementary gate signals, resulting in two switching states, i.e., insert or

bypass. The corresponding output voltage of the SM is denoted as $u_{sm,i}$, which is expressed as

$$u_{sm,i} = S_i u_{c,i}, i \in [1, 2, \dots, 2N] \quad (2)$$

where S_i is the binary switching function of the i th SM and $u_{c,i}$ is the corresponding capacitor voltage.

Open-circuit faults of the IGBTs in the MMC are a noteworthy issue due to their severe consequences. Zhou et al. [7] proposed an MBFD approach based on a model predictive control (MPC), as shown in Fig. 3. Given the known switching states by the MPC controller and the existing sensors of the MMC, the open-circuit fault is identified by checking the residual between the measurement and the estimation in the former control cycle. For example, the measured sum of the upper and lower arm voltage u_m and corresponding estimation u_e can be expressed as

$$u_m = \sum_{i=1}^{2N} u_{sm,i} = \sum_{i=1}^{2N} S_i u_{c,i} \quad (3)$$

$$u_e = U_{dc} - L_0 \left(\frac{i_p^k - i_p^{k-1}}{T_s} + \frac{i_n^k - i_n^{k-1}}{T_s} \right) \quad (4)$$

where i_p , i_n , U_{dc} , and $u_{c,i}$ are obtained from the sensors of the MMC system, L_0 is a known model parameter, and T_s is the sampling period. To enable the residual independent of the SM capacitor voltage, the normalized residual is expressed as

$$\varepsilon = \frac{N(u_m - u_e)}{U_{dc}}. \quad (5)$$

In an ideal condition, the residual $|\varepsilon|$ is zero if no fault while the one above zero is fault. To consider inevitable uncertainties, a threshold ε_{th} is typically employed and the fault is identified only when the residual satisfies $|\varepsilon| > \varepsilon_{th}$. The threshold in [7] has $\varepsilon_{th} = 0.8$. Although their experimental results have validated good effectiveness in the laboratory conditions, whether the empirical selection of the threshold performs a robust MBFD remains unknown. The subsequent part of the section will use an analytical method to analyze the uncertainties at first.

B. Analytical Investigation of the MBFD Uncertainties

To model different uncertainties, an uncertainty factor $\delta_x \in \mathbb{R}^+$ is defined as

$$\tilde{x} = \delta_x \cdot x \quad (6)$$

where \tilde{x} represents a practical value and x is the parameter without considering uncertainties. Substituting different categories of uncertainties listed in Table II, (3) and (4) can be rewritten as

$$\tilde{u}_m = \sum_{i=1}^{2N} \delta_{u_c} u_{sm,i} \quad (7)$$

$$\begin{aligned} \tilde{u}_e &= \delta_{U_{dc}} U_{dc} \\ &- \delta_{L_p} L_0 \frac{\delta_{i_p} (i_p^k - i_p^{k-1})}{T_s} - \delta_{L_n} L_0 \frac{\delta_{i_n} (i_n^k - i_n^{k-1})}{T_s}. \end{aligned} \quad (8)$$

TABLE II
DIFFERENT CATEGORIES OF UNCERTAINTY FACTORS AFFECT THE MBFD

Type	Parameter x	Practical value \tilde{x} or notes
Parameter mismatch	L_0	$\tilde{L}_p = \delta_{L_p} L_0$ $\tilde{L}_n = \delta_{L_n} L_0$
Measurement accuracy	U_{dc} u_c i_p i_n	$\tilde{U}_{dc} = \delta_{U_{dc}} U_{dc}$ $\tilde{u}_c = \delta_{u_c} u_c$ $\tilde{i}_p = \delta_{i_p} i_p$ $\tilde{i}_n = \delta_{i_n} i_n$
Varied conditions	U_{dc}, i_g	e.g., step change, load variations
System parameter	N, T_s	enhancing or attenuating uncertainties

The residual with considering uncertainties is modeled as

$$\tilde{\varepsilon} = N \frac{\tilde{u}_m - \tilde{u}_e}{\tilde{U}_{dc}}. \quad (9)$$

To understand the uncertainties behind the MBFD's residual, the residual variation between the one under ideal conditions and the one subject to uncertainties is defined as Δ_ε , which is expressed as

$$\Delta_\varepsilon = \varepsilon - \tilde{\varepsilon}. \quad (10)$$

By substituting (1), (5), and (9) into (10), the residual variation is decomposed into two parts as

$$\Delta_\varepsilon = \Delta_{\varepsilon_dc} + \Delta_{\varepsilon_ac} \quad (11)$$

where

$$\begin{aligned} \Delta_{\varepsilon_dc} &= \frac{N}{\delta_{U_{dc}} U_{dc}} \left[(\delta_{U_{dc}} - \delta_{u_c}) \sum_{i=1}^{2N} u_{sm,i} \right] \\ \Delta_{\varepsilon_ac} &= \frac{NL_0}{\delta_{U_{dc}} U_{dc}} \left[(\delta_{L_n} \delta_{i_n} - \delta_{L_p} \delta_{i_p}) \left(\frac{i_g^k - i_g^{k-1}}{2T_s} \right) \right. \\ &\quad \left. + (2\delta_{U_{dc}} - \delta_{L_p} \delta_{i_p} - \delta_{L_n} \delta_{i_n}) \left(\frac{i_{cir}^k - i_{cir}^{k-1}}{T_s} \right) \right]. \end{aligned} \quad (13)$$

Accordingly, the uncertainties of the residual consist of two parts, i.e., the biased part Δ_{ε_dc} and the fluctuated part Δ_{ε_ac} . The bias part is mainly affected by the measurement accuracy $\delta_{U_{dc}}$ and δ_{u_c} , and the fluctuated part is affected by multiple uncertainty factors, such as δ_{L_p} , δ_{L_n} , δ_{i_p} , δ_{i_n} , and $\delta_{U_{dc}}$. In addition to the steady state, the residual uncertainties also depend on the dynamics of U_{dc} and i_g , which are related to the operational conditions and the controller. Moreover, other parameters such as N and T_s also affect the residual by enhancing or attenuating uncertainties. In the next section, the case study will reveal that Δ_{ε_ac} is prone to false alarms while Δ_{ε_dc} may cause missed alarms due to weakened residual.

IV. UNCERTAINTY QUANTIFICATION BASED ON MONTE CARLO EVALUATION

The analytical model above provides qualitative understandings of the uncertainty sources, however, the analytical model

TABLE III
MAIN CIRCUIT PARAMETERS OF THE MMC FOR MONTE CARLO ANALYSIS

Parameters	Values	Units
Rated power	1.2	MW
The ac side current	100	A
The dc bus voltage	20	kV
Arm inductance	20	mH
Line frequency	50	Hz
Number of SMs per arm	10	-
SM capacitance	2000	μ F
SM capacitor voltage	2000	V
Sampling and control period	20	μ s

alone is difficult to obtain quantitative results of the uncertainty propagation, especially considering multiple uncertainty sources and operational dynamics simultaneously. To address this problem, this section employs Monte Carlo analysis to evaluate the uncertainty propagation. The nominal parameters of the analyzed MMC system are listed in Table III.

A. Random Variate Generation

According to the aforementioned analysis, the uncertainty sources are mainly from three typical categories, namely parameter mismatch, measurement accuracy, and operational variations. In our previous work [22], we introduced a method for selecting variations based on established boundaries, taking into account manufacturing tolerances, environmental conditions, distribution types, and confidence levels. In this article, the reasonable variations of selected parameters are strictly followed by practical conditions and the existing literature, which are given by the following.

- 1) *Parameter mismatch*: Inductance mismatch is selected as $\pm 20\%$ [26] to consider different factors, such as the manufacturing tolerance, the value variations along with temperature, saturation, and degradation effects. Thus, $\delta_{L_p}, \delta_{L_n} \in [0.8, 1.2]$.
- 2) *Measurement accuracy*: According to the data sheets of the state-of-the-art sensors [27], [28], [29], the high-voltage sensor typically has $\pm 3\%$ accuracy, capacitor voltage measurement has around $\pm 2\%$ accuracy, and the arm current sensing has $\pm 3\%$ accuracy. Thus, $\delta_{U_{dc}}, \delta_{i_p}, \delta_{i_n} \in [0.97, 1.03]$, $\delta_{u_c} \in [0.98, 1.02]$.
- 3) *Operational variations*: Considering the step changes of voltage or load in dynamics, U_{dc} can drop from 1 to 0.9 p.u., and i_g can change from 1 into -1 p.u. to consider the severe load variations in the operation.

The first two categories are independent random factors, which tend to be in a normal distribution according to the central limit theorem. Whereas, the operational variations are not purely random issues, which are regarded as a uniform distribution. Then, 1000 random multiparameter variations within the defined distributions are generated and their combinations are shown in Fig. 4. Two selected cases are marked in the distribution, which will be analyzed later in detail.

An important issue of Monte Carlo analysis is to determine if the number of random parameter combinations is sufficient.

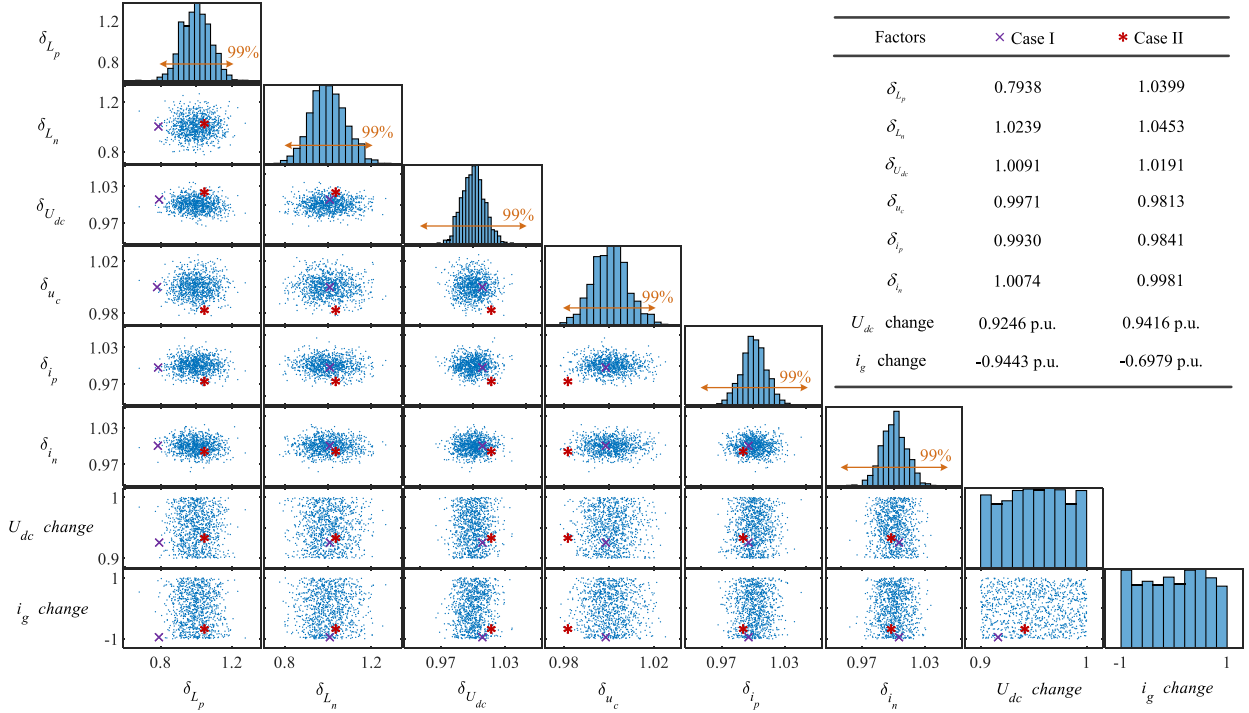


Fig. 4. Distributions of multiple uncertainty factors varying simultaneously. U_{dc} change and i_g change emulate the operational dynamics. For instance, U_{dc} change or i_g change = 0.9 p.u. means that the dc bus voltage or the ac side current have a step change from 1 p.u. to 0.9 p.u. at $t = 0.025$ s. The selected Cases I and II will be analyzed later.

The central limit theorem provides a stopping rule [30], which is expressed as

$$e_r = \frac{\Phi^{-1}\left(1 - \frac{\alpha}{2}\right) \sqrt{\frac{\sigma^2(Y)}{n}}}{\bar{Y}} \quad (14)$$

where $\Phi^{-1}(\cdot)$ is the inverse Gaussian probability distribution, $\sigma^2(\cdot)$ represents the variance, α represents the desired confidence level ($\alpha = 0.05$ means 95% confidence), Y and \bar{Y} are the output of Monte Carlo analysis and its average, and n is the total number of Monte Carlo analysis. A higher number of n tends to having a smaller analysis error. The analysis is, thus, stopped if the sample mean error e_r falls below a specified threshold. In this work, $e_r \leq 1\%$ and $\alpha = 0.05$ ensure 95% confidence that the analysis gives a relative error of less than 1%. All following provided results have been validated by this criterion.

B. Monte Carlo Analysis

To assess the performance of the MBFD method, two categories of the misdiagnosis risk are defined as Types I and II error rates, which are given by

$$\begin{aligned} \text{Type I error rate} &= \Pr(|\varepsilon| > \varepsilon_{th} | \text{Health}) \\ \text{Type II error rate} &= \Pr(|\varepsilon| \leq \varepsilon_{th} | \text{Fault}). \end{aligned} \quad (15)$$

The Type I error rate is computed as the probability where the system is in a health state but the detected outcome is faulty. In analogy, the Type II error rate is defined vice versa.

The top of Fig. 5 shows the residual distribution under health and fault states, respectively, and the middle part shows their

correspondingly selected waveforms of the two cases. To begin with, when the MMC system is under a health state (i.e., no open-circuit fault), the top left of Fig. 5 shows the residual distribution subject to different uncertainties. Although the residual is largely concentrated within the defined threshold $\varepsilon_{th} = 0.8$, there are 153 samples among the 1000 combinations above the threshold. By using a curve fitting of a generalized extreme value distribution, the Type I error rate is 14.30%, which leads to false alarms. A selected residual waveform of Case I is shown in the middle left of Fig. 5. Although the system does not have any open-circuit faults, the uncertainties cause the residual having a dc bias around 0.1 and an ac fluctuated part around 0.5. A load step change at $t = 0.025$ s enhances the residual fluctuation beyond the threshold, leading to a false alarm in this case.

On the contrary, when the MMC has an open-circuit fault, the right of Fig. 5 shows the distribution of the residual. Among the 1000 samples, 992 faults have a residual greater than the threshold of 0.8, and only 8 faults are missed in the detection. The Type II error rate is 0.30% in statistics. Similarly, the waveform of a missed alarm (Case II) is also provided. A significant dc bias of around 0.4 exists in the residual, leading to lowering the residual amplitude during the fault and preventing it from triggering the threshold. Thus, the MBFD is unable to detect the fault in this condition.

According to the abovementioned results and (15), it also can be seen that the residual that ε_{th} plays a vital role in the misdiagnosis risk. For example, increasing ε_{th} may be able to reduce the Type I error rate but at the cost of increasing the Type II error rate. Our preliminary effort [31] has utilized the proposed framework to optimize the threshold value selection

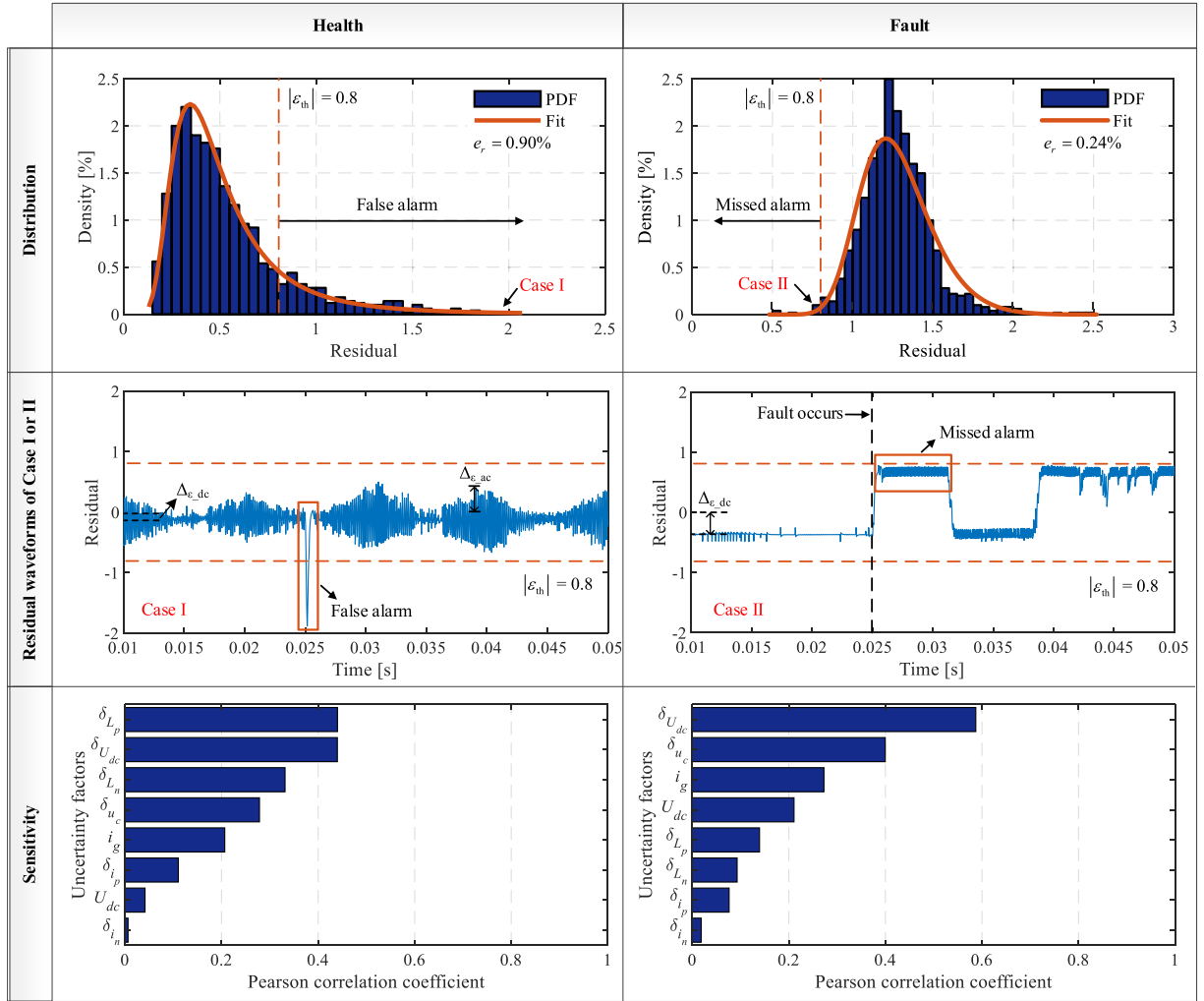


Fig. 5. Uncertainty quantification of the existing MBFD method under health and fault states. From top to bottom: MBFD's residual distribution, the residual waveforms of Case I or Case II, and their sensitivity analysis. (e_r is the sample mean error of the Monte Carlo analysis according to (14), and PDF is probability density function).

considering the two contrasting errors. However, simple shifting the threshold value is limited to improve the overall MBFD performance. Prioritizing uncertainty effects and addressing the leading factors are a promising direction to reduce the two error types simultaneously.

C. Sensitivity Analysis

The correlations between residual and uncertainty factors are computed to investigate, which factors are the leading ones. Pearson correlation coefficient ρ_{XY} , as the most common sensitivity analysis method [32] is used in this work. The inputs (X), e.g., uncertainties, are ranked by their influence on the output (Y), e.g., the residual, which is given by

$$\rho_{XY} = \frac{|\sum_{i=1}^n (X_i - \bar{X})(Y_i - \bar{Y})|}{\sqrt{\sum_{i=1}^n (X_i - \bar{X})^2 \cdot \sum_{i=1}^n (Y_i - \bar{Y})^2}} \quad (16)$$

where \bar{X} and \bar{Y} are the corresponding average values. The value of ρ_{XY} has a range from 0 to 1, where a larger value indicates a stronger correlation.

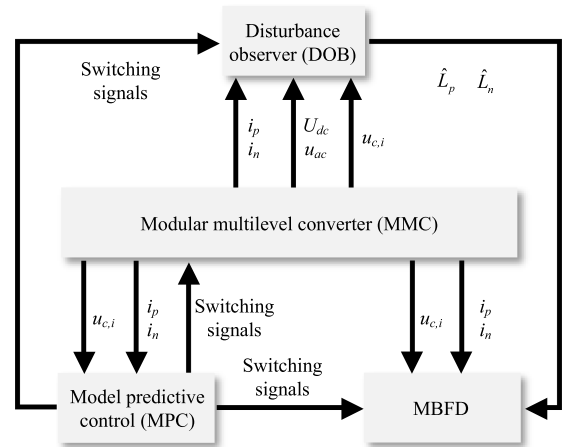


Fig. 6. Structure of the DOB-enhanced MBFD method.

The bottom of Fig. 5 shows the correlations of the residual in health and fault states, respectively. Combining analytical investigation of (12) and (13), the following conclusions can be

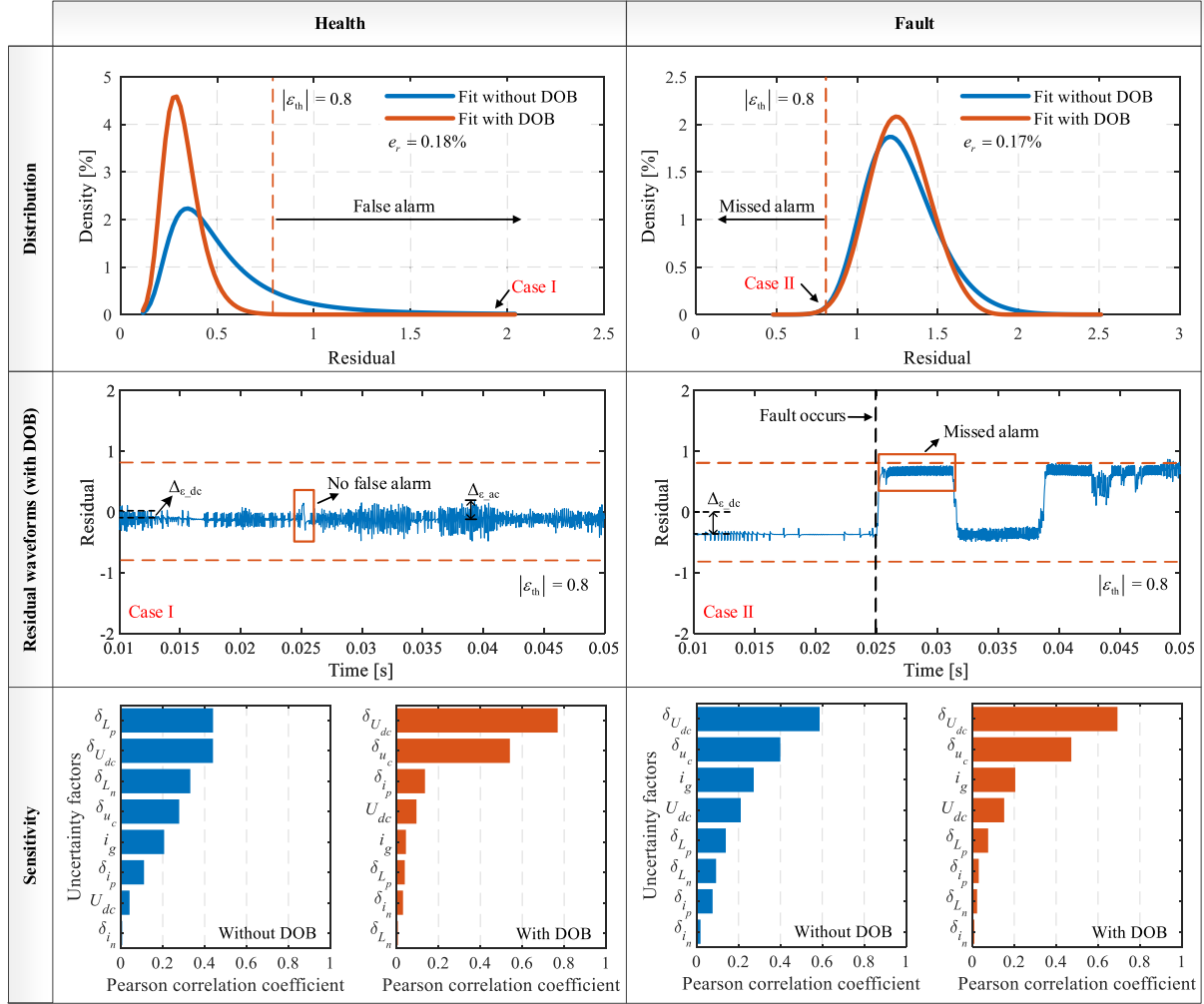


Fig. 7. Comparison of the proposed DOB-enhanced MBFD method and the conventional method under the same uncertainties distribution. From top to bottom: the residual distribution, the waveforms of Cases I and II, and their sensitivity analysis.

drawn. First, the arm inductance mismatch significantly affects the residual in health state. This parameter mismatch along with operational step change can enhance the ac fluctuation of the residual and cause false alarms. Next, the measurement accuracy in particular of $\delta_{U_{dc}}$ and δ_{u_c} plays a vital role in both health or fault states. The dc bias caused by them is more likely to lead to missed alarms since the other uncertainty factors typically tend to magnify the residual.

V. OPTIMIZATION SOLUTION: DISTURBANCE OBSERVER (DOB) ENHANCED MBFD

The aforementioned analysis reveals that inductance mismatch is one of the leading factors affecting MBFD performance, leading to false alarms. By considering this mismatch as epistemic uncertainty, which can be reduced or eliminated, the subsequent research hypothesis is that a more accurate real-time estimation of inductance can enhance the MBFD performance.

In this section, a DOB-based inductance estimation method is proposed. The real-time estimated upper and lower arm inductance \hat{L}_p and \hat{L}_n can improve the performance of the MBFD.

The uncertainty quantification is conducted again to compare the performances.

A. DOB-Based Inductance Estimation

Considering the different mismatches of inductances in the upper and lower arms, the voltage equations of upper and lower arms are normalized to be a linearized state-space model, which is described by the following:

$$\begin{cases} \mathbf{x}^{k+1} = \Phi \mathbf{x}^k + \Gamma \mathbf{u}^k + \mathbf{G} \mathbf{d}^k \\ \mathbf{y}^k = \mathbf{C} \mathbf{x}^k \end{cases} \quad (17)$$

where \mathbf{x} is the system state, \mathbf{u} is the control input, \mathbf{y} is the measured output, \mathbf{d} is regarded as the unknown value of inductance mismatch that needs to be observed, and Φ , Γ , \mathbf{G} , and \mathbf{C} are known parameter matrices, which are included in Appendix (A1)–(A4). A DOB-based inductance estimation is, thus, given by [33]

$$\begin{aligned} \hat{\mathbf{d}}^k &= [\hat{d}_1, \hat{d}_2]^T = \mathbf{K} \mathbf{x}^k - \mathbf{z}^k \\ \mathbf{z}^{k+1} &= \mathbf{z}^k + \mathbf{K}[(\Phi - \mathbf{C})\mathbf{x}^k + \Gamma \mathbf{u}^k + \mathbf{G} \hat{\mathbf{d}}^k] \end{aligned} \quad (18)$$

where $\hat{\mathbf{d}}$ is the estimated value of \mathbf{d} , \mathbf{z} is the state variable of DOB, and \mathbf{K} is the observer gain. The stability of the DOB can be achieved if $\text{rank}(\mathbf{G}) = \text{rank}(\mathbf{d})$. The specific proof can be found in [33]. Therefore, the upper and lower arm inductances can be estimated by

$$\hat{\mathbf{L}} = \begin{bmatrix} \hat{L}_p \\ \hat{L}_n \end{bmatrix} = \begin{bmatrix} \frac{1}{\frac{d_1}{U_{dc}/2 - u_{ac} - u_p} + \frac{1}{L_0}} \\ \frac{1}{\frac{d_2}{U_{dc}/2 + u_{ac} - u_n} + \frac{1}{L_0}} \end{bmatrix} \quad (19)$$

where $\hat{\mathbf{L}}$ is the estimated inductance values.

According to the proposed DOB-based inductance estimation method, the compensated estimated voltage \hat{u}_e and the corresponding normalized residual $\hat{\varepsilon}$ can be rewritten as

$$\hat{u}_e = U_{dc} - \hat{L}_p \frac{i_p^k - i_p^{k-1}}{T_s} - \hat{L}_n \frac{i_n^k - i_n^{k-1}}{T_s} \quad (20)$$

$$\hat{\varepsilon} = \frac{N(u_m - \hat{u}_e)}{U_{dc}}. \quad (21)$$

Fig. 6 shows the structure of the DOB-enhanced MBFD method. The upper and lower arm inductances are real-time estimated, respectively, to consider the individual variations.

B. Uncertainty Quantification of the DOB-Enhanced MBFD

The top of Fig. 7 shows the comparison of the residual distributions under health and fault states, respectively. For the health state, the residual distribution of the DOB-enhanced MBFD becomes more concentrated. For the 1000 Monte Carlo analysis, there is zero false alarm. The statistic Type I error rate is 0.03% only. For the fault state, although the residual distribution of the DOB-enhanced MBFD method becomes more concentrated, the Type II error rate is almost unchanged (i.e., 0.32%). Therefore, the proposed method effectively reduces the false alarm of the MBFD method.

Similarly, the residual waveforms of Cases I and II with the DOB-enhanced method are shown in the middle of Fig. 7. For the health state, the residual fluctuations are significantly suppressed by the proposed method. A further load step change at $t = 0.025$ s does not cause significant residual variation either. It reveals that mitigation of the inductance parameter mismatch can weaken the effect of operational variation.

The bottom of Fig. 7 shows the correlation coefficient change after the implementation of the DOB-enhanced method. In the health state, the DOB-enhanced method effectively reduces the rank of the inductance mismatch from the dominant factors into the last. The increased coefficients of $\delta_{U_{dc}}$ and δ_{u_c} reveal that the voltage measurement accuracy becomes more important to further improve the MBFD performance after mitigating the impact of the inductance. However, it may require better sensors, changing hardware, or compensating sensor by modeling efforts [34]. In the fault state, the rank of the different uncertainty factors remains almost unchanged after the implementation of the DOB-enhanced method.

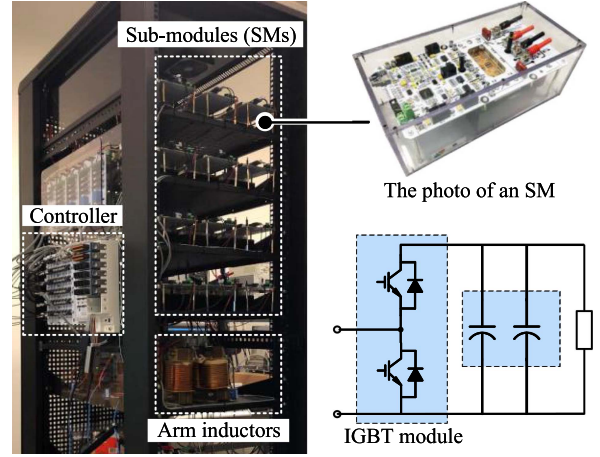


Fig. 8. 8 kVA down-scale MMC experimental prototype.

TABLE IV
MAIN CIRCUIT PARAMETERS USED IN EXPERIMENTS

Parameters	Values	Units	Descriptions
The ac side current	20	A	Nominal value
	5	A	Changed value
Arm inductance	5	mH	Nominal value
	3	mH	δ_{L_p} or $\delta_{L_n} = 0.6$
	4	mH	δ_{L_p} or $\delta_{L_n} = 0.8$
	6	mH	δ_{L_p} or $\delta_{L_n} = 1.2$
The dc bus voltage	600	V	Other factors
Number of SMs per arm	4	-	Other factors
SM capacitance	1640	μF	Other factors
SM capacitor voltage	150	V	Other factors
Sampling and control period	50	μs	Other factors

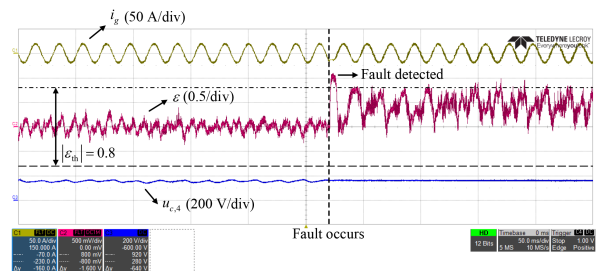


Fig. 9. Experiment result of an open-circuit fault detection by the MBFD.

VI. EXPERIMENTAL RESULTS

An 8 kVA down-scale MMC prototype has been built for experimental verification, as shown in Fig. 8. The detailed specifications are listed in Table IV. Based on the aforementioned analysis, we focus on mitigating the false alarm problem, which is mainly caused by inductance mismatch. Both steady-state and dynamic conditions are considered.

To begin with, the IGBT switch T_1 of the fourth SM in the upper arm is disabled to emulate the open-circuit fault, as shown in Fig. 9. At the occurrence of the fault, the residual suddenly

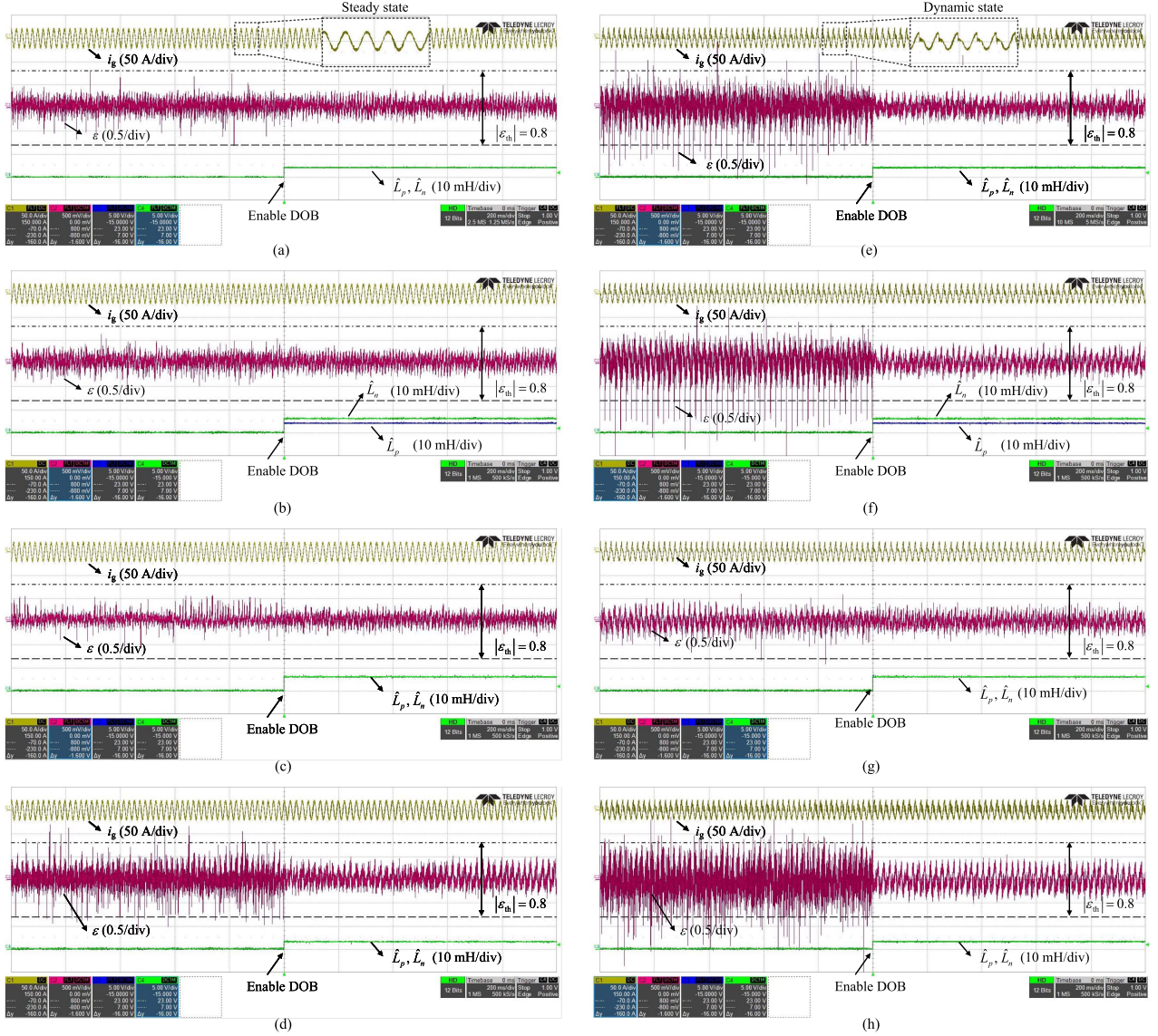


Fig. 10. MBFD's residual with different inductance mismatches. Steady state: (a) $\delta_{L_p} = \delta_{L_n} = 0.8$, (b) $\delta_{L_p} = 0.8, \delta_{L_n} = 1.2$, (c) $\delta_{L_p} = \delta_{L_n} = 1.2$, and (d) $\delta_{L_p} = \delta_{L_n} = 0.6$. Dynamic states: (e) $\delta_{L_p} = \delta_{L_n} = 0.8$, (f) $\delta_{L_p} = 0.8, \delta_{L_n} = 1.2$, (g) $\delta_{L_p} = \delta_{L_n} = 1.2$, and (h) $\delta_{L_p} = \delta_{L_n} = 0.6$.

increases and triggers the threshold $\varepsilon_{th} = 0.8$. The open-circuit fault is detected well. In the following, the system under health state is evaluated with different inductance mismatches, including both steady state and dynamics.

A. Experimental Results in Steady State and Dynamics

1) *Steady State*: Considering the arm inductance mismatch, the residual with varied arm inductance in steady state, as shown in Fig. 10(a)–(d). Four different inductance mismatches are considered, namely, $\delta_{L_p} = \delta_{L_n} = 0.8$, $\delta_{L_p} = 0.8$ while $\delta_{L_n} = 1.2$, $\delta_{L_p} = \delta_{L_n} = 1.2$, and $\delta_{L_p} = \delta_{L_n} = 0.6$. For instance, $\delta_{L_p} = \delta_{L_n} = 0.8$ means that the practical inductance is only 80% of the nominal value and others can be understood by analogy.

With $\delta_{L_p} = \delta_{L_n} = 0.8$, Fig. 10(a) shows the results. Before enabling the DOB, the residual suffers from large fluctuations. Certain peaks are beyond the defined threshold and cause false

alarms. After enabling the proposed DOB, the inductance has been accurately estimated. The fluctuation of the residual is suppressed and no false alarm anymore.

Similarly, Fig. 10(b)–(d) shows the results when the upper and lower arm inductances are divergent, undervalued, and overvalued, respectively. The inductance mismatch indeed affects the residual waveform. The proposed DOB can accurately estimate the inductance and suppress the residual fluctuations. Especially for the case with $\delta_{L_p} = \delta_{L_n} = 0.6$, the overvalued inductance causes serious false alarms with intensive residual peaks above the threshold. The proposed DOB-enhanced method can effectively mitigate these risks.

2) *Dynamics*: By intentionally introducing a load step change by changing the ac side current from 20 to 5 A periodically, Fig. 10(e)–(h) shows the MBFD performance under dynamics. Compared to the aforementioned steady state, the operational dynamics exacerbate the false alarms. They all have

TABLE V
UNCERTAINTY AND FAILURE RISK ASSESSMENT OF STATE OF THE ARTS

Ref.	Type I error (False alarm)		Type II error (Missed alarm)	
	Error rate	Leading uncertainties	Error rate	Leading uncertainties
[7]	14.30%	$\delta_{L_p}, \delta_{U_{dc}}$	0.30%	$\delta_{U_{dc}}, \delta_{u_c}$
[9]	9.41%	$\delta_{L_p}, \delta_{L_n}$	0.96%	$\delta_{U_{dc}}, \delta_{u_c}$
[35]	20.85%	δ_{L_p}, i_g	0.01%	$\delta_{u_c}, \delta_{U_{dc}}$
[36]	0.23%	$\delta_{U_{dc}}, \delta_{u_c}$	10.38%	$\delta_{U_{dc}}, \delta_{u_c}$
[37]	0.02%	$\delta_{U_{dc}}, \delta_{u_c}$	2.66%	$\delta_{U_{dc}}, \delta_{u_c}$
This article	0.03%	$\delta_{U_{dc}}, \delta_{u_c}$	0.32%	$\delta_{U_{dc}}, \delta_{u_c}$

Note: Parameter mismatch – $\delta_{L_p}, \delta_{L_n}$. Measurement accuracy – $\delta_{U_{dc}}, \delta_{u_c}$. Operational variation – i_g .

false alarms in the four cases. However, the residual can be stabilized after enabling the proposed DOB method. The influence of operational dynamics can be well suppressed by inductance estimation even under load step changes. These behaviors are identical with the results shown in the aforementioned simulation.

B. Uncertainty and Failure Risk Assessment of the Existing Methods

To highlight the impact of uncertainties on MBFD methods of power electronics systems, four additional methods [9], [35], [36], [37] are selected and evaluated based on the proposed framework. The risk-of-failure of these MBFD methods is listed in Table V. While all these studies have demonstrated the effectiveness of their methods under specific simulation or experimental conditions, uncertainties, and the risk of misdiagnosis remain prevalent in MBFD methods of power electronic systems. Some methods exhibit false alarm rates as high as 20%, which can severely disrupt the system's normal operation. Furthermore, from the results in the table, we observe that Type I errors are closely related to parameter mismatches and operational variation, while measurement accuracy significantly impacts Type II errors. The proposed DOB-enhanced MBFD method can mitigate the leading uncertainty factor and improve overall performance considering the two error rates.

VII. CONCLUSION

This article introduces a probabilistic framework for evaluating MBFD performance in power electronic systems. The framework systematically addresses uncertainty factor selection, propagation, risk assessment, sensitivity analysis, and the development of tailored solutions to optimize MBFD. Our investigation highlights several key findings.

- 1) The impact of uncertainties on MBFD residuals involves both dc bias and ac fluctuation components, with intricate interdependencies among different uncertainty factors. Addressing the leading uncertainty factors is effective to enhance the MBFD performance.
- 2) Employing two quantified error rates, the analysis demonstrates that a well-validated MBFD method from current

literature underperforms when subjected to multiple uncertainties. This highlights the limitations of conventional robustness tests based on deterministic scenarios.

- 3) Leveraging the proposed framework, we identify inductance mismatch as a leading factor impairing MBFD performance. We propose a DOB-enhanced MBFD method tailored to mitigate this uncertainty, validated through simulations and experiments demonstrating improved performance under various conditions.
- 4) Importantly, the proposed framework has evaluated six different MBFD methods from the literature and reveals their misdiagnosis rates up to 20%. This evaluation underscores the necessity of applying a probabilistic framework to assess and enhance MBFD methods for practical applications.

In conclusion, the proposed probabilistic framework not only identifies significant challenges in current MBFD methods but also provides effective strategies for improving their performances in power electronic systems.

APPENDIX

$$\mathbf{x} = \begin{bmatrix} i_p(t) \\ i_n(t) \end{bmatrix}, \mathbf{u} = \begin{bmatrix} \frac{1}{2}U_{dc} - u_{ac} - u_p \\ \frac{1}{2}U_{dc} + u_{ac} - u_n \end{bmatrix} \quad (A1)$$

$$\mathbf{d} = \begin{bmatrix} d_1 \\ d_2 \end{bmatrix} = \begin{bmatrix} (\frac{1}{L_p} - \frac{1}{L_o})(\frac{1}{2}U_{dc} - u_{ac} - u_p) \\ (\frac{1}{L_n} - \frac{1}{L_o})(\frac{1}{2}U_{dc} + u_{ac} - u_n) \end{bmatrix} \quad (A2)$$

$$\Phi = \begin{bmatrix} 1 & 0 \\ 0 & 1 \end{bmatrix}, \Gamma = \begin{bmatrix} T_s/L_o & 0 \\ 0 & T_s/L_o \end{bmatrix} \quad (A3)$$

$$\mathbf{G} = \begin{bmatrix} T_s & 0 \\ 0 & T_s \end{bmatrix}, \mathbf{C} = \begin{bmatrix} 1 & 0 \\ 0 & 1 \end{bmatrix}. \quad (A4)$$

where \tilde{L}_p and \tilde{L}_n represent their true values.

ACKNOWLEDGMENT

The authors would like to thank Prof. Huai Wang for his valuable discussions and insights, which were helpful in shaping our understanding of the topic. They also would like to thank Dr. Zhongxu Wang for contributing to the development of the experimental platform.

REFERENCES

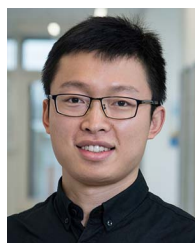
- [1] P. Jain, J. Poon, J. P. Singh, C. Spanos, S. R. Sanders, and S. K. Panda, "A digital twin approach for fault diagnosis in distributed photovoltaic systems," *IEEE Trans. Power Electron.*, vol. 35, no. 1, pp. 940–956, Jan. 2020.
- [2] Y. Zhang, H. Wang, Z. Wang, F. Blaabjerg, and M. Saeedifard, "Mission profile-based system-level reliability prediction method for modular multilevel converters," *IEEE Trans Power Electron.*, vol. 35, no. 7, pp. 6916–6930, Jul. 2020.
- [3] H. Badihi, Y. Zhang, B. Jiang, P. Pillay, and S. Rakheja, "A comprehensive review on signal-based and model-based condition monitoring of wind turbines: Fault diagnosis and lifetime prognosis," *Proc. IEEE*, vol. 110, no. 6, pp. 754–806, Jun. 2022.
- [4] F. Rojas, C. Jerez, C. M. Hack, O. Kalmbach, J. Pereda, and J. Lillo, "Faults in modular multilevel cascade converters—Part II: Fault tolerance, fault detection & diagnosis and system reconfiguration," *IEEE Open J. Ind. Electron.*, vol. 3, pp. 594–614, Oct. 2022.

- [5] B. Li, Y. Zhang, R. Yang, G. Wang, and D. Xu, "An IGBT open-circuit fault detection method for modular multilevel converters," in *Proc. 9th Int. Conf. Power Electron.*, 2015, pp. 1573–1578.
- [6] Y. Zhang, Y. Zhang, J. Zhang, F. Deng, and F. Blaabjerg, "Potential failure risk of fault location for modular multilevel converters under light loads and a current reshaping-based solution," *IEEE Trans. Power Electron.*, vol. 39, no. 3, pp. 3601–3612, Mar. 2024.
- [7] D. Zhou, S. Yang, and Y. Tang, "A voltage-based open-circuit fault detection and isolation approach for modular multilevel converters with model predictive control," *IEEE Trans. Power Electron.*, vol. 33, no. 11, pp. 9866–9874, Nov. 2018.
- [8] M. Chai, N. B. Y. Gorla, and S. K. Panda, "Fault detection and localization for cascaded h-bridge multilevel converter with model predictive control," *IEEE Trans. Power Electron.*, vol. 35, no. 10, pp. 10109–10120, Oct. 2020.
- [9] Y. Jin et al., "A novel detection and localization approach of open-circuit switch fault for the grid-connected modular multilevel converter," *IEEE Trans. Ind. Electron.*, vol. 70, no. 1, pp. 112–124, Jan. 2023.
- [10] Z. Wang and L. Peng, "Grouping capacitor voltage estimation and fault diagnosis with capacitance self-updating in modular multilevel converters," *IEEE Trans. Power Electron.*, vol. 36, no. 2, pp. 1532–1543, Feb. 2021.
- [11] D. Coronado and K. Fischer, "Condition monitoring of wind turbines: State of the art, user experience and recommendations," Fraunhofer Institute for Wind Energy and Energy System Technology, Bremerhaven, Germany, Tech. Rep., Jan. 2015, pp. 1–83. [Online]. Available: [https://www.vgb.org/vgbmultimedia/383_Final report-p-9786.pdf](https://www.vgb.org/vgbmultimedia/383_Final%20report-p-9786.pdf)
- [12] M. Rezamand, M. Kordestani, R. Cariveau, D.S.-K. Ting, and M. Saif, "A new hybrid fault detection method for wind turbine blades using recursive PCA and wavelet-based PDF," *IEEE Sensors J.*, vol. 20, no. 4, pp. 2023–2033, Feb. 2020.
- [13] F. Guan, W. Cui, L. Li, W. Xue, X. Ma, and D. Hong, "A method of false alarm recognition in built-in test considering its time series characteristics," *IEEE Trans. Ind. Electron.*, vol. 68, no. 11, pp. 11428–11437, Nov. 2021.
- [14] C. Wang, K. Pang, M. Shahidehpour, and F. Wen, "MLP-based fault diagnosis model in active power distribution networks," *IEEE Trans. Smart Grid.*, vol. 12, no. 5, pp. 3847–3857, Sep. 2021.
- [15] R. Venkataraman, P. Seiler, M. Lukátsi, and B. Vanek, "Reliability assessment of actuator architectures for unmanned aircraft," *J. Aircr.*, vol. 54, no. 3, pp. 955–966, May 2017.
- [16] D. Zhang, A. D. Bailey, and D. Djurdjanovic, "Bayesian identification of hidden Markov models and their use for condition-based monitoring," *IEEE Trans. Reliab.*, vol. 65, no. 3, pp. 1471–1482, Sep. 2016.
- [17] J. Ilonen, J.-K. Kamarainen, T. Lindh, J. Ahola, H. Kalviainen, and J. Partanen, "Diagnosis tool for motor condition monitoring," *IEEE Trans. Ind. Appl.*, vol. 41, no. 4, pp. 963–971, Aug. 2005.
- [18] J. Hu, X. Bian, Z. Wei, J. Li, and H. He, "Residual statistics-based current sensor fault diagnosis for smart battery management," *IEEE J. Emerg. Sel. Topics Power Electron.*, vol. 10, no. 2, pp. 2435–2444, Apr. 2022.
- [19] A. M. Peco Chacón, I. Segovia Ramírez, and F. P. García Márquez, "State of the art of artificial intelligence applied for false alarms in wind turbines," *Arch. Comput.*, pp. 2659–2683, Aug. 2022.
- [20] N. Rashidi, Q. Wang, R. Burgos, C. Roy, and D. Boroyevich, "Multi-objective design and optimization of power electronics converters with uncertainty quantification—Part I: Parametric uncertainty," *IEEE Trans. Power Electron.*, vol. 36, no. 2, pp. 1463–1474, Feb. 2021.
- [21] Y. Chen, A. Sangwongwanich, M. Huang, S. Pan, X. Zha, and H. Wang, "Failure risk assessment of grid-connected inverter with parametric uncertainty in LCL filter," *IEEE Trans. Power Electron.*, vol. 38, no. 8, pp. 9514–9525, Aug. 2023.
- [22] Y. Zhang, H. D. Hwang, Y. M. Gu, J. Kim, F. Blaabjerg, and H. Wang, "Physical model based Monte Carlo early failure analysis of a switching mode power supply used in HVDC transmissions," in *Proc. CIGRE Session*, 2022, pp. 1–8.
- [23] W. Zhang, Y. He, and J. Chen, "A robust open-circuit fault diagnosis method for three-level t-type inverters based on phase voltage vector residual under modulation mode switching," *IEEE Trans. Power Electron.*, vol. 38, no. 4, pp. 5309–5322, Apr. 2023.
- [24] M. Chen and Y. He, "Multiple open-circuit fault diagnosis method in NPC rectifiers using fault injection strategy," *IEEE Trans. Power Electron.*, vol. 37, no. 7, pp. 8554–8571, Jul. 2022.
- [25] C. Wang, Z. Zheng, K. Wang, and Y. Li, "Fault detection and tolerant control of IGBT open-circuit failures in modular multilevel matrix converters," *IEEE J. Emerg. Sel. Topics Power Electron.*, vol. 10, no. 6, pp. 6714–6727, Dec. 2022.
- [26] N. R. Mehrabadi, R. Burgos, C. Roy, and D. Boroyevich, "Power electronics modeling and design: Using parametric and model-form uncertainty quantification to assess predictive accuracy of power converter models," *IEEE Power Electron. Mag.*, vol. 4, no. 4, pp. 44–52, 2017.
- [27] D. A. Douglass, "Potential transformer accuracy at 60 Hz voltages above and below rating and at frequencies above 60 Hz," *IEEE Trans. Power Appar. Syst.*, vol. PAS-100, no. 3, pp. 1370–1375, Mar. 1981.
- [28] LEM, "DVC 1000," Jan. 2023. [Online]. Available: https://www.lem.com/sites/default/files/products_datasheets/dvc_1000_v3.pdf
- [29] LEM, "HAHIDRW 100-S/SP5," Oct. 2020. [Online]. Available: https://www.lem.com/sites/default/files/products_datasheets/hah1drw_s_sp5_public_v0.pdf
- [30] G. Fishman, *Monte Carlo: Concepts, Algorithms, and Applications*. New York, NY, USA: Springer-Verlag, 1996.
- [31] Y. Liao, Y. Zhang, J. You, L. Jin, Z. Xu, and Z. Shen, "Uncertainty-informed threshold assessment of model-based fault detection for modular multilevel converters," *IEEE Open J. Power Electron.*, vol. 5, pp. 802–811, May 2024.
- [32] K. N. Hasan, R. Preece, and J. V. Milanović, "Priority ranking of critical uncertainties affecting small-disturbance stability using sensitivity analysis techniques," *IEEE Trans. Power Syst.*, vol. 32, no. 4, pp. 2629–2639, Jul. 2017.
- [33] K.-S. Kim and K. H. Rew, "Reduced order disturbance observer for discrete-time linear systems," *Automatica*, vol. 49, no. 4, pp. 968–975, 2013.
- [34] D. Xie et al., "Diagnosis and resilient control for multiple sensor faults in cascaded H-bridge multilevel converters," *IEEE Trans. Power Electron.*, vol. 38, no. 9, pp. 11435–11450, Sep. 2023.
- [35] X. Chen, J. Liu, Z. Deng, S. Song, S. Du, and D. Wang, "A diagnosis strategy for multiple IGBT open-circuit faults of modular multilevel converters," *IEEE Trans. Power Electron.*, vol. 36, no. 1, pp. 191–203, Jan. 2021.
- [36] B. Li, S. Shi, B. Wang, G. Wang, W. Wang, and D. Xu, "Fault diagnosis and tolerant control of single IGBT open-circuit failure in modular multilevel converters," *IEEE Trans. Power Electron.*, vol. 31, no. 4, pp. 3165–3176, Apr. 2016.
- [37] S. Shao, P. W. Wheeler, J. C. Clare, and A. J. Watson, "Fault detection for modular multilevel converters based on sliding mode observer," *IEEE Trans. Power Electron.*, vol. 28, no. 11, pp. 4867–4872, Nov. 2013.



Yantao Liao received the Ph.D. degree in electrical engineering from Southeast University, Nanjing, China, in 2024.

He was a Visiting Scholar with Aalborg University, Aalborg, Denmark, from November 2019 to November 2021. His research interests include fault diagnosis and advanced control techniques of power electronic applications.



Yi Zhang (Member, IEEE) received the B.S. and M.S. degrees from the Harbin Institute of Technology, Harbin, China, in 2014 and 2016, respectively, and the Ph.D. degree from Aalborg University, Aalborg, Denmark, in 2020, all in electrical engineering.

He is currently an Assistant Professor with Aalborg University. During 2020–2023, he was affiliated with multiple institutions as a DFF International Post-doctoral Research Fellow, including RWTH Aachen University, Aachen, Germany, Swiss Federal Institute of Technology Lausanne, Lausanne, Switzerland, and

Massachusetts Institute of Technology, Cambridge, MA, USA. He was also a Visiting Scholar with the Georgia Institute of Technology, Atlanta, GA, USA, in 2018. His research interests include reliability of power electronics components and systems.

Dr. Zhang is currently the Guest Associate Editor for IEEE TRANSACTIONS ON POWER ELECTRONICS. He was the recipient of the First Place Prize Paper Award of the IEEE TRANSACTIONS ON POWER ELECTRONICS in 2021, and the IEEE Power Electronics Society Ph.D. Thesis Award in 2020.